IOP Publishing Journal of Physics: Condensed Matter
J. Phys.: Condens. Matter **27** (2015) 385402 (10pp) doi:10.1088/0953-8984/27/38/385402

Phonon dispersion and zero-point renormalization of $LiNbO_3$ from density-functional perturbation theory

Michael Friedrich, Arthur Riefer, Simone Sanna, W G Schmidt and Arno Schindlmayr

Department Physik, Universität Paderborn, 33095 Paderborn, Germany

E-mail: Michael.Friedrich@uni-paderborn.de

Received 18 June 2015, revised 5 August 2015
Accepted for publication 12 August 2015
Published 4 September 2015

Abstract

The vibrational properties of stoichiometric $LiNbO_3$ are analyzed within density-functional perturbation theory in order to obtain the complete phonon dispersion of the material. The phonon density of states of the ferroelectric (paraelectric) phase shows two (one) distinct band gaps separating the high-frequency ($\sim$800 cm^{-1}) optical branches from the continuum of acoustic and lower optical phonon states. This result leads to specific heat capacites in close agreement with experimental measurements in the range 0–350 K and a Debye temperature of 574 K. The calculated zero-point renormalization of the electronic Kohn–Sham eigenvalues reveals a strong dependence on the phonon wave vectors, especially near Γ. Integrated over all phonon modes, our results indicate a vibrational correction of the electronic band gap of 0.41 eV at 0 K, which is in excellent agreement with the extrapolated temperature-dependent measurements.

Keywords: lithium niobate, zero-point renormalization, lattice dynamics, ferroelectrics, phonon dispersion, electron–phonon coupling

(Some figures may appear in colour only in the online journal)

1. Introduction

Lithium niobate ($LiNbO_3$, LN, see figure 1) is a ferroelectric material with outstanding physical properties used in a wide range of technical applications. Due to its large pyroelectric, piezoelectric, acousto-optic, nonlinear, and electro-optic coefficients, it is ideally suited for applications such as optical switches, acoustic-wave transducers and filters in cellphones, motion controllers, or optical modulators and wavelength converters in fibre telecommunication systems [1]. Despite its versatility and widespread use in photonics, many properties of LN are far from being really understood.

In particular, the fundamental band gap is the subject of ongoing LN research with high significance for optical applications. While experimental values between 3.28 [2] and 4.3 eV [3] have been reported, theoretical predictions range from 2.62 eV in the single-particle scheme [4] to 6.53 eV from simplified quasiparticle calculations [5]. The discrepancies are partially related to methodological reasons [6] and partially to the sample stoichiometry [7], but in part they arise from lattice vibration effects: a temperature-dependent shift of the fundamental absorption edge by 0.5 eV was found by Redfield and Burke [7] in the range of 0–667 K. A temperature dependence was also noticed in the measured refractive indices [8, 9]. Clearly, electronic and optical excitations are affected via electron–phonon coupling.

While many experimental [10–17] and theoretical [5, 18–20] studies have been dedicated to the LN lattice vibrations, the present knowledge of the phonon modes and frequencies is essentially limited to the center of the Brillouin zone. In fact, we are aware of only a single attempt to determine the full LN phonon dispersion curves: Parlinski *et al* [19] calculated the phonon frequencies at four high-symmetry points and then approximated the dispersion using an interpolation scheme based on the crystal symmetry. Furthermore, the angular dispersion relation of extraordinary phonons at the Γ point was studied in [20].

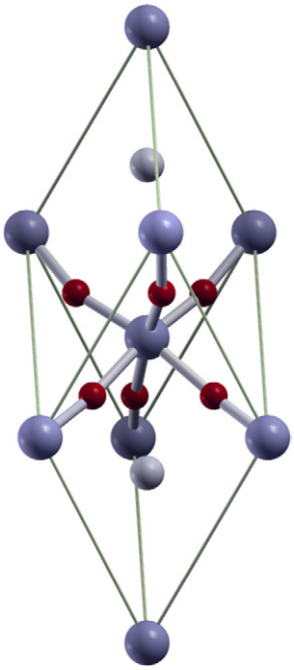

Figure 1. Ferroelectric phase of lithium niobate. The lithium (grey) and oxygen (red) atoms are displaced along the three-fold vertical axis. Niobium atoms are displayed in blue.

Table 1. Reduced hexagonal coordinates of the LN atomic basis.

	Ferroelectric	Paraelectric
Li	$\left(0, 0, \frac{1}{4} + z\right)$	$\left(0, 0, \frac{1}{4}\right)$
Nb	(0, 0, 0)	(0, 0, 0)
O	$\left(-\frac{1}{3} + v, -\frac{1}{3} - u, \frac{7}{12} - w\right)$	$\left(-\frac{1}{3} + x, -\frac{1}{3}, \frac{7}{12}\right)$
O	$\left(\frac{1}{3} + u, u + v, \frac{7}{12} - w\right)$	$\left(\frac{1}{3}, x, \frac{7}{12}\right)$
O	$\left(-u - v, \frac{1}{3} - v, \frac{7}{12} - w\right)$	$\left(-x, \frac{1}{3} - x, \frac{7}{12}\right)$
Li	$\left(0, 0, \frac{3}{4} + z\right)$	$\left(0, 0, \frac{3}{4}\right)$
Nb	$\left(0, 0, \frac{1}{2}\right)$	$\left(0, 0, \frac{1}{2}\right)$
O	$\left(\frac{1}{3} - u - v, \frac{1}{3} - u, \frac{5}{12} - w\right)$	$\left(\frac{1}{3} - x, \frac{1}{3}, \frac{5}{12}\right)$
O	$\left(-\frac{1}{3} + u, -v, \frac{5}{12} - w\right)$	$\left(-\frac{1}{3}, -x, \frac{5}{12}\right)$
O	$\left(v, -\frac{1}{3} + u + v, \frac{5}{12} - w\right)$	$\left(x, -\frac{1}{3} + x, \frac{5}{12}\right)$

The present work has two aims: first, we extend the knowledge of the LN lattice vibrations by an accurate quantitative calculation of the complete phonon dispersion over the first Brillouin zone from *first principles* via density-functional perturbation theory (DFPT). Instead of interpolating, we compute the phonon modes individually on a fine mesh throughout the first Brilloiun zone, which leads to notable changes in the dispersion compared to less elaborate previous studies. These phonon frequencies allow for an excellent reproduction of the measured specific heat at temperatures up to 350 K. Second, we analyze the impact of vibronic effects on the electronic band structure by determining the zero-point renormalization (ZPR) within DFPT. Our results are validated by a frozen-phonon calculation in which we evaluate the ZPR independently at five phonon wave vectors for comparison. By integrating over all phonon modes we ultimately obtain a *first-principles* value for the zero-point correction of the electronic band gap, which agrees well with a value that we extract from experimental measurements of the fundamental absorption edge [7].

2. Computational method

Our calculations are performed within density-functional theory (DFT) [21, 22] as implemented in the ABINIT package [23–25]. The lattice dynamics are calculated within density-functional perturbation theory [26–29]. The electron exchange and correlation interaction is described by the local-density approximation (LDA) as parametrized by Perdew and Zunger [30] as well as the generalized gradient approximations (GGA) by Perdew, Burke, and Ernzerhof (PBE) [31], by Perdew *et al* (PBEsol) [32], and by Armiento and Mattsson (AM05) [33]. The PBEsol and AM05 functionals are known to closely reproduce the experimental lattice constants [34], which is important for an accurate evaluation of the interatomic forces and thus the phonon frequencies. In contrast, LDA lattice constants are usually 1–2% too small, while PBE typically yields 1–2% larger lattice constants compared to experimental values. The electron-ion interaction is modeled using optimized norm-conserving Vanderbilt pseudopotentials [35]. Thereby, the 1*s* and 2*s* orbitals of lithium, the 2*s* and 2*p* orbitals of oxygen, and the 4*s*, 4*p*, 4*d*, and 5*s* orbitals of niobium are treated as valence states.

A plane-wave basis set defined by a kinetic cut-off energy of 46 Hartree and a Monkhorst-Pack [36] mesh of $4 \times 4 \times 4$ **k** points in the first Brillouin zone lead to energies that are converged within 1×10^{-5} Hartree. The atomic positions are determined using the effective Broyden–Fletcher–Goldfarb–Shanno minimization scheme [37] until the Hellmann–Feynman forces drop below 5×10^{-7} Hartree/Bohr. While the calculation of the phonon band structure and displacements is sampled on a $4 \times 4 \times 4$ **q**-point mesh and converged within $1\,\mathrm{cm}^{-1}$, far more **q** points are required to obtain converged results for the ZPR.

The lattice contribution to the specific heat capacity per unit cell at constant volume, given by

$$C_\mathrm{V} = 3nk_\mathrm{B} \int \left(\frac{\hbar\omega}{2k_\mathrm{B}T}\right)^2 \mathrm{csch}^2\left(\frac{\hbar\omega}{2k_\mathrm{B}T}\right) g(\omega)\,\mathrm{d}\omega, \qquad (1)$$

is calculated here from the phonon density of states $g(\omega)$ determined on a $15 \times 15 \times 15$ **q**-point mesh and using a $5\,\mathrm{cm}^{-1}$ frequency interval width, which leads to a numerical error below 0.1%. The symbol n denotes the number of atoms per unit cell.

Table 2. Calculated LN lattice parameters in comparison to experimental data for the ferroelectric phase at 300 K and the paraelectric phase at 1500 K and to previous calculations.

Ferroelectric phase	a Å^{-1}	c Å^{-1}	u	v	w	z
LDA	5.060	13.707	0.0130	0.0273	0.0177	0.0337
PBE	5.194	14.030	0.0094	0.0378	0.0202	0.0317
PBEsol	5.149	13.860	0.0111	0.0355	0.0187	0.0325
PBEsol ($\Omega^{\mathrm{PE}}_{\mathrm{expt}}$)	5.251	14.050	0.0088	0.0480	0.0193	0.0328
AM05	5.171	13.902	0.0103	0.0387	0.0191	0.0323
Expt. ([45])	5.151	13.876	0.0095	0.0383	0.0192	0.0329
Theory ([20])	5.067	13.721	0.0125	0.0302	0.0183	0.0350
Theory ([5])	5.161	13.901	0.0121	0.0278	0.0191	0.0339

Paraelectric phase	a Å^{-1}	c Å^{-1}	x
LDA	5.116	13.595	0.039
PBE	5.231	13.817	0.047
PBEsol	5.199	13.688	0.046
PBEsol ($\Omega^{\mathrm{PE}}_{\mathrm{expt}}$)	5.285	13.869	0.055
AM05	5.215	13.712	0.048
Expt. ([45])	5.289	13.848	0.060
Theory ([20])	5.125	13.548	0.042
Theory ([5])	5.219	13.756	0.041

Note: PBEsol ($\Omega^{\mathrm{PE}}_{\mathrm{expt}}$) denotes calculations that were performed at the unit-cell volume measured at 1500 K.

The $\mathbf{q}$-dependent zero-point renormalization $\Delta\epsilon^{\mathrm{ZPR}}_{n\mathbf{k}}(\mathbf{q})$ of the electronic Kohn–Sham eigenvalues is computed using both a finite-difference technique [38] as well as the DFPT implementation of the Allen, Heine and Cardona (AHC) theory [39, 40] in ABINIT [41, 42]. Within a $8\times8\times8$ $\mathbf{q}$-point mesh we achieve an error bar of, on average, 0.007 eV and at most 0.033 eV for the electronic eigenvalues $\epsilon_{n\mathbf{k}}$. To restrict the high computational effort but nevertheless take the strong $\mathbf{q}$-point dependence near Γ properly into account, we use 98 additional $\mathbf{q}$ points close to the Brillouin-zone center, corresponding locally to a $16\times16\times16$ $\mathbf{q}$-point mesh, which reduces the maximum error to 0.015 eV. In case of the finite-difference method, the ZPR is obtained from the second-order derivative of the electronic eigenvalues $\epsilon_{n\mathbf{k}}$ with respect to the amplitude h of the phononic displacements

$$\Delta\epsilon^{\mathrm{ZPR}}_{n\mathbf{k}}(\mathbf{q}) = \frac{1}{2}\sum_{j=1}^{3n}\frac{\hbar}{2\omega_j(\mathbf{q})}\frac{\partial^2}{\partial h^2} \times\epsilon_{n\mathbf{k}}[\{\mathbf{R}^{(0)}_{l,\kappa}+h\mathbf{U}_{j,\kappa}(\mathbf{q})\mathrm{e}^{-\mathrm{i}\mathbf{q}\cdot\mathbf{R}_l}\}]\Big|_{h=0}, \quad (2)$$

where $\omega_j(\mathbf{q})$ is the frequency of phonon mode j, $\mathbf{U}_j$ is the normalized phonon eigendisplacement vector of the j'th phonon mode [38], l is the number of the unit cell and κ the index of the atom. $\mathbf{R}_l$ is a lattice vector and $\mathbf{R}^{(0)}_{l,\kappa}$ a vector to the equilibrium position of atom κ. To evaluate the curvature, we fit $\epsilon_{n\mathbf{k}}(h=0)$ and $\epsilon_{n\mathbf{k}}\left(h=5\sqrt{m_{\mathrm{e}}}\ \mathrm{Bohr}\right)$ to a parabolic curve. This choice of h leads to displacements of about 4×10^{-3} Å. For illustrative purposes, we compute the ZPR for five different $\mathbf{q}$ points in the first Brillouin zone. Earlier studies [38, 43, 44] suggest a strong $\mathbf{q}$-point dependence of the ZPR for the electronic eigenenergies in solids such as diamond, which we find here as well for the case of LN.

3. Results

3.1. Structure optimization

$LiNbO_3$ is a member of the trigonal crystal system. Its uniaxial unit cell contains 10 atoms, i.e. two formula weights per primitive (rhombohedral) unit cell. Below 1480 K, LN is ferroelectric and occurs in the $R3c$ space group ($3m$ crystallographic group). At the Curie temperature it undergoes a structural phase transition to the more symmetric $R\bar{3}c$ space group ($-3m$ crystallographic group). Figure 1 shows the primitive rhombohedral unit cell. As rhombohedral coordinates are less descriptive, we list the atomic positions in reduced hexagonal coordinates in table 1. In this setting, two primitive vectors $(-\sqrt{3}\ a/2, a/2, 0)$ and $(0, -a, 0)$ lie in the xy plane, while the third vector $(0, 0, c)$ points along the z direction. a and c are the hexagonal lattice parameters. The internal parameters u, v, w, z for the ferroelectric phase and x for the paraelectric phase are degrees of freedom of the respective symmetry group and determined during the relaxation. The optimized lattice parameters are given in table 2 and compared to neutron powder-diffraction measurements at 300 K for the ferroelectric phase and at 1500 K for the paraelectric phase [45], as well as earlier calculations within LDA by Veithen and Ghosez [20] and within GGA-PW91 [46, 47] by Schmidt *et al* [5].

As expected, the PBEsol and AM05 functionals perform best in the ferroelectric case, while, similar to earlier calculations [5, 20], PBE and LDA over- and underestimate the

experimental lattice constants, respectively. For the internal lattice parameters the agreement is generally much better, except that LDA yields a notably too small value for v. Interestingly, [5] and [20] also reported very small theoretical values for v.

For the paraelectric phase, no functional is able to predict the experimentally observed lattice constants. This is not surprising, because DFT is a ground-state theory that does not take thermal expansion into account. Furthermore, the internal parameter x, which plays the same role as v in the ferroelectric phase, is consistently underestimated. PBE shows the best overall agreement with [45] due to a cancellation of errors. In order to simulate the effect of thermal expansion, we perform an additional relaxation of the unit cell and the atomic positions, i.e. the internal parameter x, with the unit-cell volume Ω kept at the experimental value at 1500 K [45]. The corresponding results are denoted as $\Omega^{\mathrm{PE}}_{\mathrm{expt}}$. In this case, not only the lattice constants a and c, but also the parameter x turn out to be very close to the experimental values. Apparently, the other theoretical results underestimate the internal parameter x due to the too small theoretical volume.

As there is no indication of a volume change during the phase transition [48], we also use the same value $\Omega^{\mathrm{PE}}_{\mathrm{expt}}$ that was measured for the paraelectric phase at 1500 K to determine the structure of ferroelectric LN at elevated temperatures. With the volume fixed at $\Omega^{\mathrm{PE}}_{\mathrm{expt}}$, we optimize the lattice constants a and c as well as all internal parameters. Consistent with our results for x in the paraelectric phase, we observe a notable increase of the internal parameter v in this scenario.

3.2. Phonons at Brillouin-zone center

The transversal optical (TO) phonon frequencies at Γ calculated here for the ferroelectric phase are presented in table 3. We compare our results to the Raman measurements of nearly stoichiometric LN crystals at room temperature by Margueron *et al* [12], which are in good agreement with [10, 13–17]. As there are only a few measurements of the silent A_2 modes, we compare these frequencies to data by Chowdhury *et al* [11] obtained from neutron scattering.

Overall, the calculated frequencies are in very good agreement with the available measurements. The deviations from the available experimental phonon frequencies at the Γ point that occur for the various functionals tested here are visualized in figure 2. We observe a slight but systematic underestimation of, on average, 4.0% for PBEsol and 5.2% for AM05 compared to [12]. Our results are consistent with the recent findings of He *et al* [49] concerning DFPT phonon calculations with several exchange-correlation functionals, who found that phonon calculations within DFPT systematically underestimate phonon frequencies and concluded that LDA gives the best results due to a cancellation of errors (too small lattice parameters lead to higher phonon frequencies), while PBEsol and AM05 perform slightly worse. Larger deviations were noticed for the PBE functional. This is essentially in accord with the present findings. However, possibly related to the limited accuracy of the LDA values for the internal parameters, especially v, we observe both over- and underestimations of phonon frequencies within LDA. The systematic frequency underestimation within PBEsol and AM05 in comparison to the less systematic behavior of the LDA values eases analysis of subsequent results derived from the calculated phonon dispersion curves. Furthermore, for the calculation of the electronic eigenvalues it is favorable to have the correct lattice parameters of the system. For this reason, the LDA, like PBE, is not used in the calculations described below.

Table 3. Calculated TO zone-center frequencies for the ferroelectric phase compared to earlier theoretical results and experimental measurements.

	Present theory		Earlier theory		
Mode	PBEsol	AM05	Reference [20]	Reference [5]	Expt.
A_1	239	241	243	238	253[a]
	272	263	288	279	277[a]
	335	326	355	350	334[a]
	607	611	617	605	632[a]
A_2	213	212	218	212	224[b]
	287	281	297	298	314[b]
	397	390	412	406	
	441	438	454	443	455[b]
	876	875	892	868	
E	148	147	155	147	155[a]
	217	219	218	216	240[a]
	257	255	264	260	265[a]
	317	306	330	321	322[a]
	352	335	372		364[a]
	364	347	384	384	370[a]
	418	415	428	421	433[a]
	570	566	585	573	580[a]
	662	662	677	662	660–667[c]

[a] Reference [12].
[b] Reference [11].
[c] Reference [12], congruent LN.

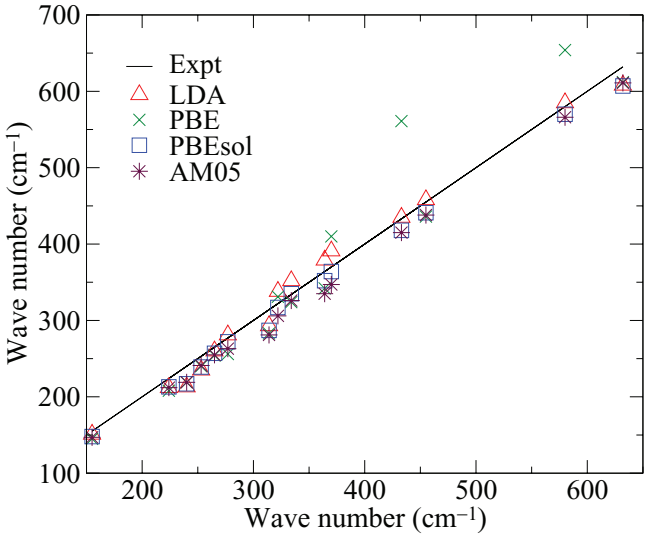

Figure 2. Deviations of the theoretical phonon frequencies at Γ for four functionals from experimental data.

Table 4. Calculated A_1 and E LO zone-center frequencies for the ferroelectric phase compared to earlier theoretical results and experimental measurements.

	Present theory		Earlier theory	Expt.
Mode	PBEsol	AM05	Reference [20]	Reference [12]
A_1	272	263	287	276
	332	325	348	334[a]
	403	404	413	421
	839	836	855	871
E	198	185	197	199
	222	222	224	241
	290	285	298	298
	334	323	349	343
	364	347	384	370
	410	402	423	426
	438	434	452	457
	660	659	675	659[a]
	846	845	863	879

[a] congruent LN.

On the theoretical side, our results can be compared with previous DFPT calculations by Veithen *et al* [20] and with data obtained from a frozen-phonon approach by Schmidt and co-workers [5], see table 3. The slight deviations observed with respect to these previous calculations may in part arise from the implementation of the different methods but are mainly due to different lattice parameters employed in the calculations. This is illustrated by the fact that our results for the PBEsol exchange-correlation functional are close to those of [5], where very similar lattice parameters were used, despite the different computational approach. On the other hand, the low value of v determined in [5] causes some deviations from the present data, similar to the findings of Veithen *et al* [20], who also obtained a small v.

In addition to the TO frequencies, we list our calculated longitudinal optical (LO) phonon frequencies in table 4. The latter are distinct at the zone center, because the macroscopic electric field of ionic crystals splits the infrared-active A_1 and E modes. Consequently, they are calculated here by adding a term to the dynamical matrix using the Born effective charges $Z^*_{\kappa,\beta\alpha}$ [29]. These are defined, at linear order, as the proportionality coefficients

$$Z^*_{\kappa,\beta\alpha} = \Omega \frac{\partial P^{\mathrm{mac}}_{\beta}}{\partial \tau_{\kappa\alpha}(\mathbf{q}=\mathbf{0})}\bigg|_{\varepsilon=0} \tag{3}$$

between the macroscopic polarization per unit cell $\mathbf{P}^{\mathrm{mac}}$ in the direction β and the displacement τ of the sublattice κ along the direction α when no external macroscopic electric field ε is present, and are calculated here within DFPT. The direction-dependent interaction of the phononic lattice distortions with the polarization gives rise to increased longitudinal frequencies.

In agreement with experiments and earlier calculations, essentially no LO–TO splitting is observed for the second A_1 mode and the sixth E mode in table 3, which correspond to the first and fifth mode in table 4, respectively. This identification is concluded from the high overlap of the respective polarization vectors for the LO and TO phonons that amounts to 95% (A_1) and 100% (E) in agreement with Hermet *et al* [50].

Table 5. Calculated zone-center frequencies of the paraelectric phase compared to earlier theoretical results.

	Present theory			Earlier theory	
Mode	PBEsol	PBEsol ($\Omega^{\mathrm{PE}}_{\mathrm{expt}}$)	AM05	Reference [20]	Reference [5]
A_{1g}	379	334	369	403	406
A_{1u}	273	262	271	279	283
	418	386	411	435	432
A_{2g}	104i	91i	101i	115i	92i
	404	404	407	405	410
	873	846	870	889	868
A_{2u}	198i	203i	202i	201i	183i
	79	31	59	94	47
	468	454	464	478	476
E_g	170	161	169	175	204
	409	345	398	425	436
	471	433	459	501	481
	569	525	560	589	578
E_u	78i	133i	103i	53i	18
	182	195	185	177	207
	382	336	378	393	384
	424	363	403	460	443
	519	484	508	532	533

Table 5 contains the values for the paraelectric phase. The frequencies obtained are in good agreement with two earlier theoretical studies in [5, 20], which also obtained smaller values for a, c, and x than experimentally determined. Unfortunately, there are no phonon measurements at 1500 K. We observe a significant change of the frequencies between the theoretical and the experimental volume. However, there is no uniform drop of the frequencies due to the larger volume. Rather, the calculations show that some frequencies decrease, while others remain unchanged or even rise, which might be caused by the change of the parameter x and the c/a ratio. Although some frequencies for $\Omega^{\mathrm{PE}}_{\mathrm{expt}}$ show sizeable deviations from previous theoretical results, we consider the present values to be more reliable, since the lattice expansion has not been taken into account previously.

The presence of imaginary frequencies confirms that the model representing the paraelectric phase and belonging to the point group $R\bar{3}c$ is an energetic saddle point, even at the experimental volume corresponding to 1500 K. Indeed, recent *ab initio* calculations have revealed that the paraelectric phase is the time average of a random distribution of Li ions above and below the oxygen planes with an average zero net polarization [51, 52]. Our results support this picture.

In agreement with [20], we find an unstable lowest E_u mode at Γ for the paraelectric phase, whereas no unstable E_u modes at Γ are reported in [19], similar to the findings of Schmidt *et al* [5] and our own test calculations with LDA and GGA Troullier-Martins [53] pseudopotentials. Evidently, the stability of the E_u modes depends sensitively on the choice of pseudopotentials and the details of the calculations. This is

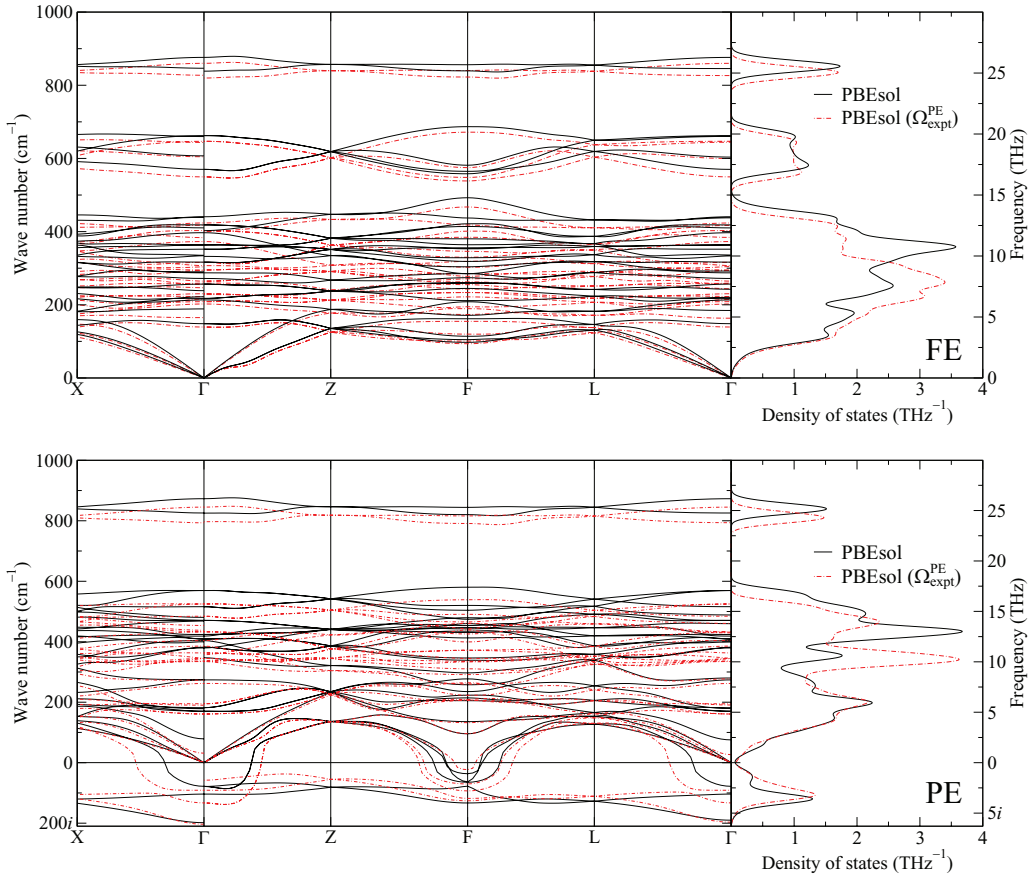

Figure 3. Phonon dispersion and density of states of ferroelectric (top) and paraelectric (bottom) $LiNbO_3$ computed with the PBEsol exchange-correlation functional.

supported by ground-state calculations with a displacement of the atoms along the unstable E_u modes that indicate only a very small diminuation of the total energy, which is in the range of numerical inaccuracies.

3.3. Phonon dispersion

Among the exchange-correlation functionals considered in section 3.2, we find PBEsol to provide the closest agreement with the experimental data for phonon modes at the center of the Brillouin zone. Therefore, PBEsol is used for the phonon dispersion calculations described below. We also mention that He *et al* [49] concluded that PBEsol generally performs better than AM05 when phonon frequencies are calculated at the experimental lattice constants. The phonon dispersion curves of both the ferroelectric and the paraelectric phase are displayed in figure 3 together with the corresponding densities of states. As thermal expansion plays a role in thermodynamic calculations, we also show the phonon dispersion curves calculated for the expanded lattice corresponding to $T = 1500$ K, denoted PBEsol (Ω^{PE}_{expt}) in figure 3. It is not suprising that the latter frequencies are generally lower than those at the theoretical volume, because the forces that arise from the phononic displacement are smaller at higher volumes. However, the phonon frequencies do not drop uniformly, as can be seen, for instance, by the branches around 350 cm^{-1} and near Γ. The reason for this are the internal parameters, which also change as a consequence of the volume expansion.

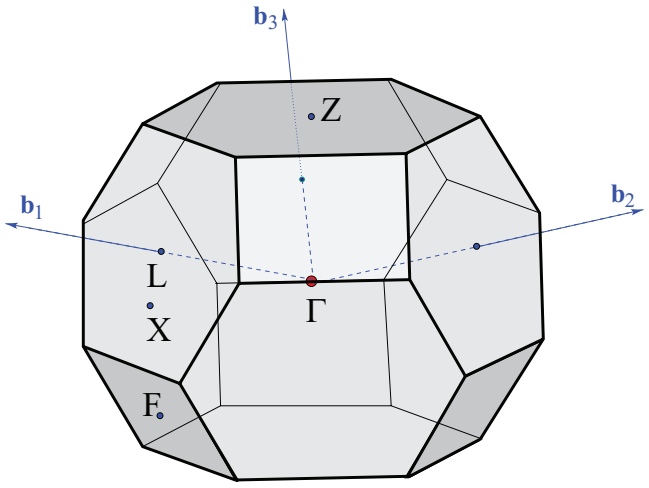

Figure 4. Brillouin zone of the rhombohedral lattice with primitive reciprocal lattice vectors $\mathbf{b}_1\left(\frac{-1}{a}, \frac{-1}{\sqrt{3}\,a}, \frac{1}{c}\right)$, $\mathbf{b}_2\left(\frac{1}{a}, \frac{-1}{\sqrt{3}\,a}, \frac{1}{c}\right)$ and $\mathbf{b}_3\left(0, \frac{2}{\sqrt{3}\,a}, \frac{1}{c}\right)$.

Figure 4 illustrates the notation used here for the rhombohedral Brillouin zone, where the path X–Γ–Z–F–L–Γ is

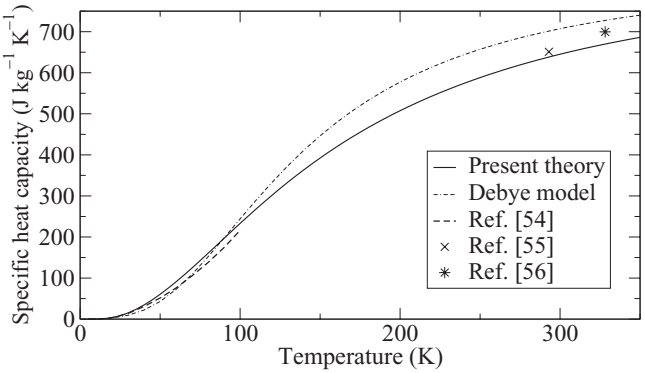

Figure 5. Theoretical results for the specific heat capacity compared to experimental measurements and to the Debye model. The Debye temperature of 574 K is determined from a fit to the calculated curve.

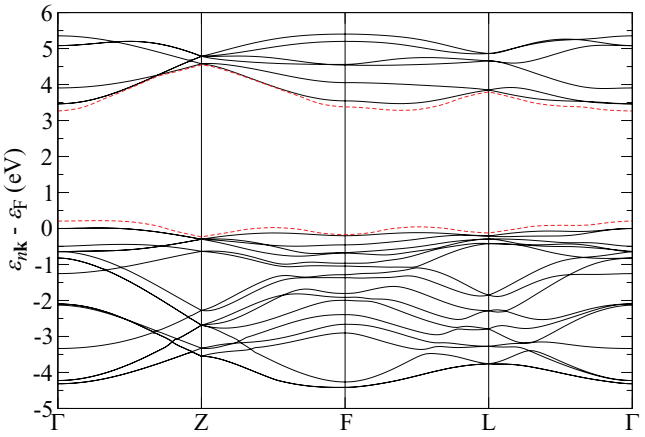

Figure 6. Calculated DFT-PBEsol band structure of LN using the theoretical lattice constants. The dashed line marks the zero-point renormalization of the highest valence and lowest conduction band(s).

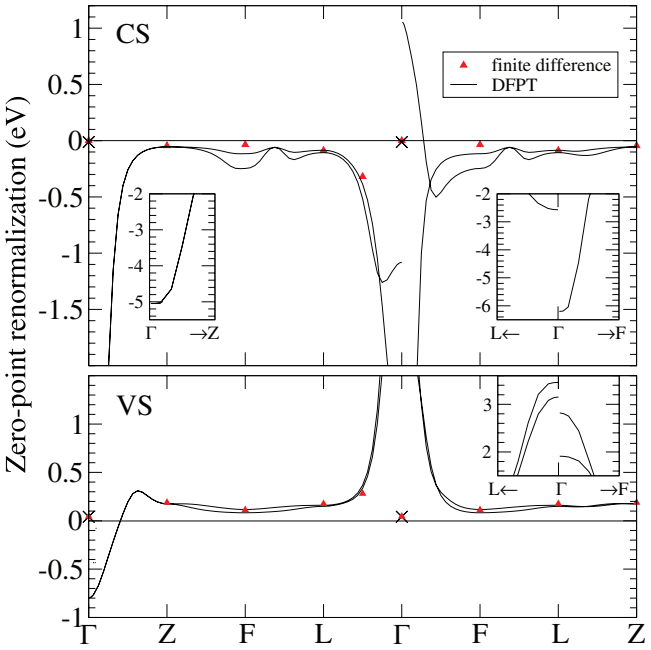

Figure 7. Zero-point renormalization of the two highest degenerate valence states (bottom) and the lowest degenerate conduction states (top) at Γ for different phonon wave vectors in the first Brillouin zone.

chosen for plotting the phonon band structure, in accord with Parlinski *et al* [19], who used the Hellmann–Feynman forces and the direct method to calculate the phonon frequencies at four high-symmetry **q** points and performed an interpolation in between, which exploits the symmetry of the crystal. For both phases in figure 3 we observe two phonon branches around 850 cm^{-1}. The four (partly degenerate) branches around 600 cm^{-1} in the ferroelectric phase drop by about 100 cm^{-1} when LN becomes paraelectric. This leads to two phonon band gaps in the dispersion for ferroelectric lithium niobate and one larger gap for paraelectric LN. The results of Parlinski *et al* differ from ours in that the dispersion of the phonon bands is generally much stronger. The width of the uppermost phonon bands calculated in [19], for example, is about five times larger than found here. Furthermore, there is nearly no gap separating the branches in [19], in marked contrast to the present findings. This might be an artifact of their interpolation scheme. In particular, we obtain similar phonon bands as in [19] if we restrict the **q**-point sampling to a coarse $2 \times 2 \times 2$ mesh. At the transition from the ferroelectric to the paraelectric phase the branches around 600 cm^{-1} drop significantly. The higher symmetry of the paraelectric phase leads to more degenerate modes at Z. The calculated dispersion further shows that imaginary frequencies occur not only at Γ, but at all wave vectors throughout the Brillouin zone.

3.4. Specific heat capacity

The present calculations of the specific heat capacity C_V at constant volume according to equation (1) are compared with experimental data in figure 5. Measurements of the specific heat capacity C_p at constant pressure for a nearly stoichiometric sample in the temperature range of 4.2–100 K were made with an automatic adiabatic calorimeter with a reported accuracy below 1% [54]. Furthermore, differential scanning calorimeters were used to determine C_p at room temperature (651 J kg^{-1} K^{-1}, stoichiometric LN) [55] and at 328.15 K (699.5 J kg^{-1} K^{-1}, nearly stoichiometric LN) [56]. In [57] a general error estimate of 1.5% is given for this technique. As the authors of [55, 56] report higher heat capacities for stoichiometric than for congruent LN, we do not take other measurements [58] into account here, because the samples contained a high concentration of lattice defects or a high impurity content [54].

We find the specific heat capacity calculated here to be in very good agreement with the experimental data. The small deviations in the lower temperature range might be explained by the fact that the sample in [54] was not entirely stoichiometric. Furthermore, the measurements were done at constant pressure rather than constant volume, whereas we do not take distinct volume effects for solids into account. For higher temperatures our lower phonon frequencies might lead to smaller values of C_p than in [55, 56]. Nevertheless, the deviations from the two experimental values are only 1.5%

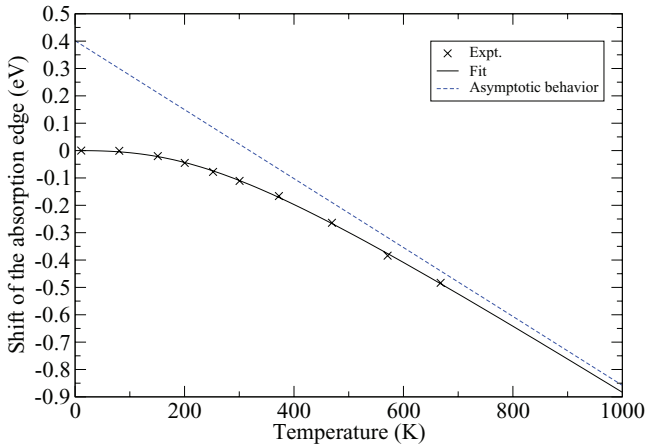

Figure 8. Experimental measurements of the fundamental absorption edge by Redfield *et al* [7] fitted to equation (5). The linear asymptote, which cannot be extracted accurately from the limited experimental data, determines the ZPR at 0 K.

and 4.2%, respectively. This is a clear, albeit indirect, indication for the reliability of the phonon dispersion curves presented here.

We further extract a Debye temperature of $T_D = 574$ K from our theoretical C_V data by fitting the calculated curve to the formula derived from the Debye model

$$C_V = 9nk_B\left(\frac{T}{T_D}\right)^3 \int_0^{T_D/T} \frac{x^4 e^x}{(e^x - 1)^2}\,dx \qquad (4)$$

between 0–10 K. This numerical result agrees very well with the value of 593 K reported by Villar *et al* [54] based on the asymptote of their experimental data for C_p. By construction, the Debye model (4) exhibits the correct limiting behavior at low and high temperatures, and figure 5 shows that it stays reasonably close to the *ab initio* curve, and consequently also to the experimental measurements, if the value T_D extracted from the theoretical data is used. Of course, it differs from the *ab initio* curve for intermediate temperatures due to its model character.

3.5. Zero-point renormalization

We next examine the size of the zero-point renormalization of the electronic energies due to the electron-phonon coupling and its dependence on the phonon wave vector. For this purpose we perform both DFPT and finite-difference calculations in order to compare these two approaches. Looking at the DFT band structure in figure 6, we notice that the electronic bands are very flat, especially the upper valence bands. The band gap is direct and located at Γ.

In figure 7 we present $\Delta\epsilon^{ZPR}_{n\mathbf{k}}(\mathbf{q})$ for the band-edge states at Γ. The two highest degenerate valence bands and the two lowest degenerate conduction bands are displayed. The corrections to the electronic eigenstates are of considerable size, up to about 6 eV, and depend strongly on the phonon wave vector **q**. Even their signs vary. For the flat valence bands, the ZPR is generally higher than for the more dispersive conduction bands, because the occurrence of flat bands leads to phonon-induced intraband transitions involving two electronic states that are separated by the corresponding phononic energy. This introduces a high, diverging electron–phonon coupling for $\mathbf{q} \to \mathbf{0}$. The same holds for the **q** vectors between F and L, where the electronic energies are roughly the same as at Γ. However, for $\mathbf{q} \cong \mathbf{0}$, the electron–phonon coupling almost vanishes, because no intraband transitions are possible in this case, and the phonon energy cannot account for interband transitions.

The strong **q**-point dependence of the ZPR, especially around Γ, indicates that an accurate knowledge of the phonon band structure is required for reliable predictions of the influence of electron–phonon coupling on the LN electronic properties. With the introduction of a finer **q**-point sampling near Γ as described above we account for the variation in this region.

The agreement between the two computational methods, i.e. the finite-difference and the DFPT approach, is very good. Differences at F reveal two weaknesses of the finite-difference approach: first, the phononic displacements break the symmetry of the crystal. As a consequence, originally degenerate or quasi-degenerate states split and thereby complicate or even impede the accurate calculation of the electron phonon coupling elements from the second derivatives of the electronic eigenvalues in equation (2). Second, it is not possible to relate the change of the electronic eigenvalues to a particular degenerate band. Fortunately, we are able to solve the latter problems for most **k** points by averaging the ZPR of degenerate states. References [44, 59] have taken advantage of this procedure before. The (linear and quadratic) splitting terms thus cancel out and the problem the assignment of the corrections is resolved. In the case of the F point, if a the $2 \times 2 \times 1$ supercell is used, the electronic bands at F are folded back to Γ. In this way, we effectively obtain triply degenerate electronic conduction states that split by the phonon displacement. Taking the average of the three states leads to incorrect results, because the former F-point conduction state produces different electron–phonon coupling elements.

The total zero-point renormalization of the band-edge states is shown in figure 6. While the band gap remains direct at Γ, the ZPR reduces the gap by 0.41 eV. The main contribution from the phonon modes comes from the second highest mode, i.e. an *E* mode, which leads to a distortion of the oxygen octahedra and affects the band-edge states arising from O 2*p* and Nb 4*p* [60], as Nb is situated inside the octahedra. Its magnitude is comparable to the sum of the other 29 phonon modes.

For comparison, we estimate the ZPR from the temperature-dependent data in [7]. Evidently, the ZPR cannot be measured directly, but it can be concluded from isotope substitution or the asymptotic linear behavior for of the temperature-dependent shift of the electronic band gap for $T \gg T_D$ [61]. Data for the latter is available from Redfield *et al* [7], who determined the shift of the fundamental absorption edge in the range of 0–667 K. The measurements are confined to this range due to the broadening of the optical spectra for higher temperatures. As suggested in [61, 62], we fit the experimental values to the empirical expression

$$\Delta E_g(T) = -\frac{\alpha T_D}{2}\left[\left(1 + \left(\frac{2T}{T_D}\right)^p\right)^{1/p} - 1\right] \qquad (5)$$

with adjustable parameters α, p, and T_D. We extract the ZPR from equation (5) by extrapolating the linear behavior for $T \gg T_D$ and thus obtain a zero-point renormalization of the electronic band gap of $\alpha T_D/2 = 0.40$ eV with $\alpha = 1.259\,29$ meV K^{-1}, $p = 2.570\,23$, and $T_D = 637.466$ K. It is recommended to use the Debye temperature T_D as a fitting parameter to obtain the best results (see figure 8) [62]. The same method was used by Cardona [63] to extrapolate the ZPR of germanium and silicon from measurements of the absorption edge, also within a limited temperature range. Moreover, these results were in very good agreement with those concluded from the isotopic effect. The agreement between our theoretical value of the ZPR for LN and the one extrapolated from the experiment is excellent. However, we note that both values are affected by uncertainties due to the missing self-energy effects in DFT [44, 59], and the fitting procedure, respectively. We estimate that the error bars are of the order of 0.1 eV in both cases.

4. Conclusions

We have performed density-functional theory calculations for the structural properties and phonon band structure of $LiNbO_3$, and the accuracy of the LDA as well as the PBE, PBEsol, and AM05 exchange-correlation functionals concerning lattice constants and phonon frequencies was tested. We found that, in particular, PBEsol provides lattice constants and internal parameters close to experiment for the ferroelectric phase as well as reliable phonon frequencies at Γ. Furthermore, we calculated the full phonon dispersions for both phases at the theoretical equilibrium volume as well as the experimental unit-cell volume at 1500 K and determined an internal parameter x for the paraelectric phase close to experimental measurements. The results for the specific heat capacity as a function of the temperature validate the results of the phonon dispersion in the first Brillouin zone. We have also shown that the zero-point renormalization of the electronic band-structure energies is large and depends strongly (even in sign) on the phonon wave vector. Our well converged result for the zero-point renormalization of the electronic band gap of $LiNbO_3$ of 0.41 eV is in excellent agreement with the value 0.40 eV determined from the temperature-dependent shift of the fundamental absorption edge in [7].

Acknowledgments

All the calculations were performed at the Paderborn Center for Parallel Computing (PC^2). We gratefully acknowledge financial support by the Deutsche Forschungsgemeinschaft (DFG) via Sonderforschungsbereich TRR 142.

References

[1] Weis R S and Gaylord T K 1985 *Appl. Phys.* A **37** 191
[2] Jiangou Z, Shipin Z, Dingquan X, Xiu W and Guanfeng X 1992 *J. Phys.: Condens. Matter* **4** 2977
[3] Kase S and Ohi K 1974 *Ferroelectrics* **8** 419
[4] Ching W Y, Gu Z-Q and Xu Y-N 1994 *Phys. Rev.* B **50** 1992
[5] Schmidt W G, Albrecht M, Wippermann S, Blankenburg S, Rauls E, Fuchs F, Rödl C, Furthmüller J and Hermann A 2008 *Phys. Rev.* B **77** 035106
[6] Thierfelder C, Sanna S, Schindlmayr A and Schmidt W G 2010 *Phys. Status Solidi* C **7** 362
[7] Redfield D and Burke W J 1974 *J. Appl. Phys.* **45** 4566
[8] Hobden M V and Warner J 1966 *Phys. Lett.* **22** 243
[9] Schlarb U and Betzler K 1993 *Phys. Rev.* B **48** 15613
[10] Barker A S and Loudon R 1967 *Phys. Rev.* **158** 433
[11] Chowdhury M R, Peckham G E and Saunderson D H 1978 *J. Phys.* C **11** 1671
[12] Margueron S, Bartasyte A, Glazer A M, Simon E, Hlinka J, Gregora I and Gleize J 2012 *J. Appl. Phys.* **111** 104105
[13] Ridah A, Bourson P, Fontana M D and Malovichko G 1997 *J. Phys.: Condens. Matter* **9** 9687
[14] Schwarz U T and Maier M 1997 *Phys. Rev.* B **55** 11041
[15] Repelin Y, Husson E, Bennani F and Proust C 1999 *J. Phys. Chem. Solids* **60** 819
[16] Claus R, Borstel G, Wiesendanger E and Steffan L 1972 *Z. Naturforsch.* A **27a** 1187
[17] Yang X C, Lan G X, Li B and Wang H F 1987 *Phys. Status Solidi* B **142** 287
[18] Caciuc V, Postnikov A V and Borstel G 2000 *Phys. Rev.* **61** 8806
[19] Parlinski K, Li Z Q and Kawazoe Y 2000 *Phys. Rev.* B **61** 272
[20] Veithen M and Ghosez P 2002 *Phys. Rev.* B **65** 214302
[21] Hohenberg P and Kohn W 1964 *Phys. Rev.* **136** B864
[22] Kohn W and Sham L J 1965 *Phys. Rev.* **140** A1133
[23] Gonze X *et al* 2005 *Z. Kristallogr.* **220** 558
[24] Gonze X *et al* 2009 *Comput. Phys. Commun.* **180** 2582
[25] Marques M A L, Oliveira M J T and Burnus T 2012 *Comput. Phys. Commun.* **183** 2272
[26] Baroni S, Giannozzi P and Testa A 1987 *Phys. Rev. Lett.* **58** 1861
[27] Zein N E 1984 *Fiz. Tverd. Tela* **26** 3024
Zein N E 1984 *Sov. Phys.—Solid State* **26** 1825
[28] Gonze X 1997 *Phys. Rev.* B **55** 10337
[29] Gonze X and Lee C 1997 *Phys. Rev.* B **55** 10355
[30] Perdew J P and Zunger A 1981 *Phys. Rev.* B **23** 5048
[31] Perdew J P, Burke K and Ernzerhof M 1996 *Phys. Rev. Lett.* **77** 3865
[32] Perdew J P, Ruzsinszky A, Csonka G I, Vydrov O A, Scuseria G E, Constantin L A, Zhou X and Burke K 2008 *Phys. Rev. Lett.* **100** 136406
[33] Armiento R and Mattsson A E 2005 *Phys. Rev.* B **72** 085108
[34] Haas P, Tran F and Blaha P 2009 *Phys. Rev.* B **79** 085104
[35] Hamann D R 2013 *Phys. Rev.* B **88** 085117
[36] Monkhorst H J and Pack J D 1976 *Phys. Rev.* B **13** 5188
[37] Schlegel H B 1982 *J. Comput. Chem.* **3** 214
[38] Poncé S, Antonius G, Gillet Y, Boulanger P, Laflamme Janssen J, Marini A, Côté M and Gonze X 2014 *Phys. Rev.* B **90** 214304
[39] Allen P B and Heine V 1976 *J. Phys.* C **9** 2305
[40] Allen P B and Cardona M 1981 *Phys. Rev.* B **23** 1495
[41] Boulanger P 2010 *PhD Thesis* Université de Montréal, Montral, Canada, and Université Catholique de Louvain, Louvain-la-neuve, Belgium
[42] Gonze X, Boulanger P and Côté M 2011 *Ann. Phys., Lpz.* **523** 168
[43] Poncé S, Antonius G, Boulanger P, Cannuccia E, Marini A, Côté M and Gonze X 2014 *Comput. Mater. Sci.* **83** 341
[44] Antonius G, Poncé S, Boulanger P, Côté M and Gonze X 2014 *Phys. Rev. Lett.* **112** 215501
[45] Boysen H and Altorfer F 1994 *Acta Crystallogr.* B **50** 405
[46] Perdew J P and Wang Y 1986 *Phys. Rev.* B **33** 8800
[47] Perdew J P, Chevary J A, Vosko S H, Jackson K A, Pederson M R, Singh D J and Fiolhais C 1992 *Phys. Rev.* B **46** 6671
[48] Abrahams S C, Levinstein H J and Reddy J M 1966 *J. Phys. Chem. Solids* **27** 1019

[49] He L, Liu F, Hautier G, Oliveira M J T, Marques M A L, Vila F D, Rehr J J, Rignanese G-M and Zhou A 2014 *Phys. Rev.* B **89** 064305
[50] Hermet P, Veithen M and Ghosez P 2007 *J. Phys.: Condens. Matter* **19** 456202
[51] Phillpot S R and Gopalan V 2004 *Appl. Phys. Lett.* **84** 1916
[52] Sanna S and Schmidt W G 2012 *IEEE Trans. Ultrason. Ferroelectr. Freq. Control* **59** 1925
[53] Troullier N and Martins J L 1991 *Phys. Rev.* B **43** 1993
[54] Villar R, Gmelin E and Grimm H 1986 *Ferroelectrics* **69** 165
[55] Nakamura M, Sekita M, Takekawa S and Kitamura K 2006 *J. Cryst. Growth* **290** 144
[56] Yao S, Wang J, Liu H, Hu X, Zhang H, Cheng X and Ling Z 2008 *J. Alloys Compd.* **455** 501
[57] Rudtsch S 2002 *Thermochimica Acta* **382** 17
[58] Lawless W N 1976 *Phys. Rev.* B **14** 134
[59] Faber C, Boulanger P, Attaccalite C, Cannuccia E, Duchemin I, Deutsch T and Blase X 2015 *Phys. Rev.* B **91** 155109
[60] Riefer A, Sanna S, Schindlmayr A and Schmidt W G 2013 *Phys. Rev.* B **87** 195208
[61] Cardona M 2001 *Phys. Status Solidi* A **188** 1209
[62] Pässler R 2003 *Phys. Status Solidi* B **236** 710
[63] Cardona M 2005 *Solid State Commun.* **133** 3